PeerJ Materials Science

The influence of thermal treatments on the secondary structure of silk fibroin scaffolds and their interaction with fibroblasts

Tomoko Hashimoto[1,2], Yuka Nakamura[2], Yasushi Tamada[1,3], Hiromichi Kurosu[2] and Tsunenori Kameda[1,4]

[1] Silk Materials Research Unit, National Institute of Agrobiological Sciences, Tsukuba, Ibaraki, Japan
[2] Faculty of Human Life and Environment, Nara Women's University, Nara, Nara, Japan
[3] Faculty of Textile Science and Technology, Shinshu University, Ueda, Nagano, Japan
[4] Silk Materials Research Unit, National Agriculture and Food Research Organization, Tsukuba, Ibaraki, Japan

ABSTRACT

Background. Recently, silk fibroin-based biomaterials have received attention for application in tissue engineering and drug delivery systems. The usefulness of heat sterilization methods for silk fibroin-based biomaterials was investigated in this study as all biomaterials are required to undergo a sterilization process when they are used in medical devices.

Methods. The influence of wet and dry heating on the properties of fibroin molecules in silk fibroin sponges was investigated by measurements of solid-state ^{13}C cross-polarization/magic angle spinning (CP/MAS) nuclear magnetic resonance (NMR) spectroscopy, thermogravimetric analyses, strength tests, and cell proliferation/migration assays.

Results. ^{13}C CP/MAS NMR spectra of wet-heated sponges revealed no changes in the molecular structure below 50 °C. However, above 60 °C, the crystalline structure of the silk proteins transitioned from silk I to silk II; the silk II:silk I ratio increased with temperature. In contrast, dry heating (below 190 °C for up to 180 min) induced no structural changes in the fibroin molecules. These results indicate that, although autoclave sterilization (121 °C for 20 min) induces structural changes in silk fibroin sponges, no such changes are observed with the dry-heat sterilization (180 °C for 30 min). Sterilized sponges with a silk I structure can be obtained using dry-heat method during sterilization. Moreover, the structural differences between the wet- and dry-heated silk fibroin sponges did not influence their interaction with fibroblasts.

Discussion. This study indicates that both autoclaving and dry heating are acceptable sterilization methods for silk fibroin-based sponges as the scaffold. In particular, dry heating maintains the stability of the secondary structure of the sterilized silk fibroin-based biomaterials.

Subjects Biomaterials, Nano and Microstructured Materials, Polymers, Porous Materials
Keywords Silk fibroin, Biomaterials, Sterilization, Protein secondary structure

Submitted 9 March 2020
Accepted 23 June 2020
Published 1 September 2020

Corresponding author
Tomoko Hashimoto,
hashitomo@cc.nara-wu.ac.jp

Academic editor
Andre Fajardo

Additional Information and Declarations can be found on page 14

DOI **10.7717/peerj-matsci.8**

How to cite this article Hashimoto T, Nakamura Y, Tamada Y, Kurosu H, Kameda T. 2020. The influence of thermal treatments on the secondary structure of silk fibroin scaffolds and their interaction with fibroblasts. *PeerJ Materials Science* **2**:e8 http://doi.org/10.7717/peerj-matsci.8

INTRODUCTION

Bombyx mori silk fibroin is a fibrillary, highly crystalline protein that is commercially used as a textile fiber because of its mechanical strength, hygroscopicity, luster and smooth texture. It has also long been used in surgical sutures, which causes no significant side effects. Recently, many reports have described the use of silk fibroin-based biomaterials in tissue engineering (*Kawakami et al., 2011*; *Lee et al., 2017*; *Luetchford, Chaudhuri & De Bank, 2020*) and drug delivery systems (*Mao et al., 2018*; *Cheng et al., 2020*) and as substrates for anticoagulants (*Tamada, 2003*) and anti-HIV materials (*Yavuz et al., 2019*). Regenerated silk fibroin can be fabricated into various forms such as films (*Aznar-Cervantes et al., 2019*), hydrogels (*Zuluaga-Vélez et al., 2019*), sponges (*Tamada, 2005*), resins (*Kaneko et al., 2012*), fibers (*Zhang et al., 2016*) and nanofibers (*Kopp et al., 2020*). A silk fibroin sponge (SFS) is a porous 3-D structure composed of silk fibroin. One of the authors reported the development of an original method for preparing SFSs (*Tamada, 2005*). Our SFS could possibly be used as a tissue engineering scaffold because its porous surface structures and mechanical properties are suitable for cell growth and handling. In general, the surface structure of biomaterials is known to affect the biological functions of cells. It is already known that surface structure has profound effects on the biological functions of the cells seeded on that surface (*Hu et al., 2011*; *Min et al., 2006*). The surface structures of fibroin materials are related to the secondary structures of silk I and silk II. Moreover, the mechanical properties of fibroin materials are also dependent on the secondary structure of fibroin. Therefore, understanding the relationships between the secondary structures of silk fibroin-based biomaterials and cellular behavior is important for the development of silk fibroin-based biomaterials. Previous studies have reported that random coils and silk I structures are transformed into silk II structures by external stimuli, such as temperature (*Hu et al., 2011*; *Tretinnikov & Tamada, 2001*), pH (*Zhou et al., 2004*; *Matsumoto et al., 2006*), ions (*Jiang & Zhou, 2011*) and organic solvents (*Jeong et al., 2006*).

Sterilization of biomaterials is crucial if they are to be used for medical procedures, and various physical, chemical and thermal methods exist for this purpose (*Noah et al., 2002*; *Holy et al., 2000*; *Marreco et al., 2004*). Physical sterilization methods, such as the exposure to gamma or UV radiation, produce excellent results without leaving behind any unwanted residues. However, high-energy radiation alters the polymers by both cross-linking and chain scission (*Holy et al., 2000*; *Bat et al., 2008*; *Archodoulaki et al., 2011*). Chemical sterilization methods, including exposure to gaseous ethylene oxide (EOG), are performed without heat treatment, and this method is suitable for temperature- and water-sensitive biomaterials. The major disadvantage of this method, however, is the requirement to remove toxic residues after treatment. Previously, one of the authors suggested that the secondary structure of the silk fabric protein produced by hornet (*Vespa*) larvae was unchanged even after being subjected to dry-heat treatment (up to 180 °C) (*Kameda & Aratani, 2011*). The molecular structures of hornet silk and silk fibroin are dissimilar. However, if silk fibroin were as heat-resistant as hornet silk and if it could maintain the silk I structure in hot dry air at 180 °C (for over 30 min), then dry-heating sterilization could also be applied to silk fibroin-based materials. Another thermal method (autoclaving)

involves heat treatment with water vapor at high temperature and pressure. Autoclaving is a simple, effective and reliable way of killing microorganisms without leaving residues. However, since autoclave procedures require high temperatures, most biopolymer-based biomaterials cannot withstand this treatment; for example, collagen is denatured by autoclaving (*Voggenreiter et al., 1994*). Native silk fibroin fibers and degummed raw silk can be sterilized by autoclaving because they are both resistant to high temperatures owing to their silk II-rich structures. However, other silk fibroin-based materials, such as sponges and films (but not fibers), respond differently to autoclaving because of the presence of a thermally unstable form of silk (silk I) or because of an abundance of random coils. Several reports have shown that water-based heat treatment adversely affects the structure of fibroin molecules (*Hu et al., 2011*; *Tretinnikov & Tamada, 2001*; *Magoshi et al., 1979*) and that the thermal stability of the secondary structure of silk fibroin varies with water content (*Hu et al., 2011*; *Hu, Kaplan & Cebe, 2008*). The effects of various types of sterilization techniques on silk fibroin-based materials, such as lamellar structures, solutions, films and nanofibers, have also been investigated (*Oliveira et al., 2012*; *Sionkowska & Planecka, 2011*; *George et al., 2013*; *Fan et al., 2012*; *Hattori et al., 2011*; *Lawrence et al., 2008*).

To facilitate use of our SFS as a tissue engineering scaffold, we investigated the influence of thermal treatments on the secondary structures of their fibroin molecules in order to assess them as potential sterilization methods. Both wet- and dry-heat treatments were investigated. Moreover, in order to examine the influence of structural changes on the interaction of cells with the SFSs, we measured the cell proliferation and motility of fibroblasts on heat-treated SFSs.

MATERIALS & METHODS

Preparation of silk fibroin sponge (SFS)

Silk fibroin aqueous solutions were prepared from the degummed silk thread of Bombyx mori by dissolution in 9 M LiBr, followed by dialysis against pure water, and SFSs were fabricated as described previously (*Tamada, 2005*; *Kameda, Hashimoto & Tamada, 2011*). Briefly, 1% v/v of DMSO (the sponge formation reagent) was added to the fibroin aqueous solution (6% w/v) and mixed thoroughly. The mixture was then poured into a mold (thickness, two mm), and the solution was placed at −20 °C and kept at this temperature for 17 h using a thermoregulated bath (EYELA, Tokyo, Japan). The mold was then thawed to room temperature to yield a porous structure. The SFSs were then washed with pure water in order to remove DMSO and subsequently stored in water at 4 °C until needed. Some SFSs were freeze-dried and sputter-coated with gold for field emission scanning electron microscopy (FESEM) imaging using JSM-6700F (JEOL, Tokyo, Japan).

Heat treatments

Wet-heating treatments were performed by immersing the SFSs (5.0 × 3.3 cm) in ion-exchanged water at predetermined temperatures (37 °C, 50 °C, 60 °C, 80 °C and 95 °C) for 360 min. Wet-heating treatments at 95 °C were also carried out for various other durations (3, 5, 10, 20, 90 and 180 min). For autoclaving, SFSs were heated to 120 °C (at a pressure of 0.11 MPa for 20 min) in ion-exchanged water using an autoclave (TOMY, Tokyo, Japan).

Table 1 Comparison of heat-treatment method.

Treatments	Temperature (°C)	Time (min)	Pressure	Abbreviation of sponges
Non-treating	–	–	–	NON
Wet-heating	37, 50, 60, 80	360	atmosphere	–
	95	3, 5, 10, 20, 90, 180, 360	atmosphere	–
Autoclaving	121	20	0.11 (MPa)	AC
Dry-heating	180	30	atmosphere	DH

Dry-heating treatment involved oven-based heating (SANYO, Tokyo, Japan) at 180 °C for 30 min. Prior to dry-heating treatments, the SFSs were dried at 25 °C for at least 12 h using a dryer equipped with a vacuum pump (YAMATO, Tokyo, Japan). These conditions are summarized in Table 1. The abbreviations used in this paper are the following: NON, non-treated SFSs; AC, autoclaved SFSs; and DH, dry-heated SFSs.

^{13}C CP/MAS NMR measurements

High-resolution solid-state ^{13}C NMR spectra were recorded on a Bruker Avance 600 WB NMR spectrometer (Bruker, Karlsruhe, Germany) equipped with a magnetic field of 14.1 T. The spectrometer was operated at a ^{13}C NMR frequency of 150.94 MHz. A 4.0 mm ϕ zirconia rotor was used as the sample tube, and magic angle spinning (MAS) was performed at a speed of 10.0 kHz. In cross-polarization (CP) experiments, a ^{1}H $\pi/2$ pulse length of 3.5 μs and a ^{1}H-^{13}C CP contact of 70 kHz were employed. The repetition time was set at 3.0 s. High-power ^{1}H decoupling was employed by the SPINAL-64 method. Approximately 16,000 scans were accumulated for each spectrum to attain a reasonable S/N ratio. The chemical shifts of all spectra were calibrated through the adamantane CH_2 peak (29.5 ppm) relative to the tetramethylsilane (TMS) peak (0 ppm).

Thermogravimetry

Weight losses as a function of temperature were measured using a thermogravimetric (TG) apparatus (Rigaku, Tokyo, Japan). Non-treated SFSs were heated from room temperature to the given temperature at a rate of 3 °C/min using uniform air flow (200 mL/min). Weight loss as a function of time of non-treated SFSs at various temperatures were measured.

Mechanical properties

The mechanical properties of the SFSs were measured using an EZ test (Shimadzu Corp., Kyoto, Japan) with a 50 N load cell. SFSs in the wet state (thickness: around two mm) were cut into a dumbbell shape and stretched with a head speed of five mm/min. The force at break is generally evaluated as the tensile strength (N/m^2) by converting it into the force per unit cross-sectional area. However, because the wet SFSs contain many voids including water, it is difficult to accurately determine the cross-section of only SFS. Therefore, using the samples with identical thickness and width, the observed values of force at break were directly used for comparison. Statistical analysis was performed to compare mechanical properties using ANOVA and the Tukey Post Hoc test ($n = 4$).

Cell culture

Cell adhesion and proliferation experiments on/in heat-treated SFSs were performed using the NIH/3T3 murine fibroblast cell line. NIH/3T3 cells were grown in Eagle's medium (EMEM; Nissui, Japan) containing 10% FBS (Invitrogen, Life Technologies Corp., USA), 2 mM L-glutamine (Invitrogen, Life Technologies Corp., USA) and 0.1 mg/mL kanamycin (Invitrogen, Life Technologies Corp., USA) in a humidified incubator (5% CO2 and 95% air at 37 °C).

Wet heating or dry heating was carried out before the cells were introduced onto the sponge surface. Prior to cell seeding, six mm diameter circles were cut from ACs using a biopsy punch and placed in EMEM for 1 h at 37 °C. DHs were first immersed in PBS before excision of six mm circles. And then, PBS was replaced with EMEM. NIH/3T3 cells were then seeded at a density of 1×10^5 cells/sponge. After 1, 24, 72, 120 and 168 h of incubation at 37 °C and 5% CO2, wells were washed with PBS to remove non-adherent cells, and 0.5% Triton X-100 in PBS was added to each well to permeabilize the cells. Lactate dehydrogenase (LDH) activity in each well was measured as described previously (*Tamada & Ikada, 1994*). The cell number at each time point was determined by comparison to a standard curve of cell number versus LDH activity and then averaged. The doubling times of the cells on the surfaces were calculated by exponential curve-fitting.

Cell migration

Cell migration experiments were performed using silk fibroin-coated glass to mimic the surface for sponges. Silk fibroin-coated glass was prepared using cover slips (15 mm in diameter, Thermo Fisher Scientific K.K., Japan) and by incubation in a fibroin aqueous solution that had been adjusted to 1% (w/v). After incubation for 30 min at room temperature, the fibroin solution was removed, and the fibroin surfaces were dried in an oven at 50 °C (for AC-mimicking surfaces) or at room temperature (for DH-mimicking surfaces) for at least 12 h. In order to induce the structural changes from random to β-sheet (*Min et al., 2004*), the AC-mimicking surfaces were treated with 80% MeOH solution for 30 min at room temperature and then dried at 50 °C for at least 12 h. Additionally, some AC-mimicking surfaces were autoclaved and treated with 70% EtOH solution for 1 h. The DH-mimicking surfaces were vacuum-dried at 25 °C for at least 12 h and then dry-heated in an oven at 180 °C for 30 min. The secondary structures of these mimicking surfaces were measured using FTIR spectroscopy (FT/IR-4100, JASCO, Tokyo, Japan) equipped with an ATR unit (PRO450-S, JASCO, Tokyo, Japan) to determine whether these surfaces did indeed mimic sponges. FTIR-ATR spectra of mimicking surfaces were recorded at a resolution of four cm^{-1} between 500 and 4,000 cm^{-1}. The contact angles of the mimicking surfaces were measured using the sessile drop method. Prior to cell culture experiments, the AC-mimicking surfaces were autoclaved for 20 min at 120 °C and then immersed in 70% v/v ethanol. Quantitative evaluations of cell migration on the mimicking surfaces were performed using the MtrackJ software as described previously (*Hashimoto et al., 2013*). Cell motility on various surfaces was averaged between five individual cells.

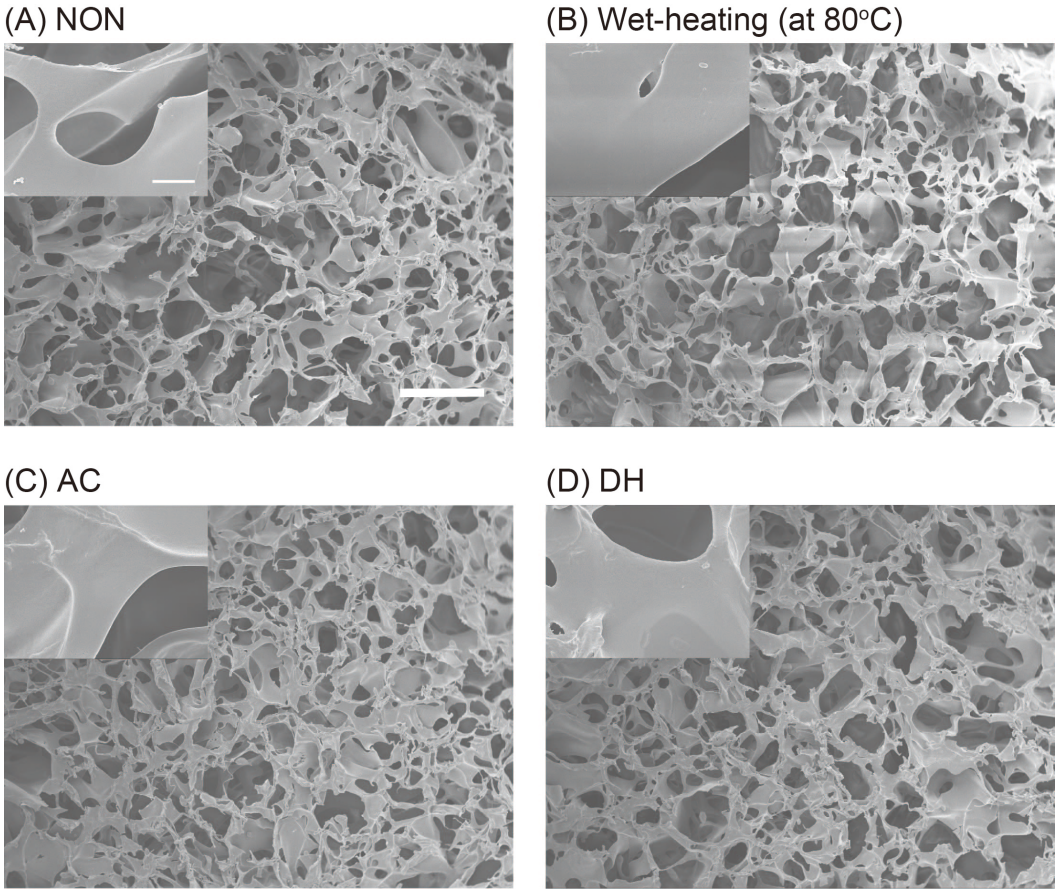

Figure 1 The morphology of SFSs. FESEM images of SFSs before heat-treatment (NON; A), and after wet-treatment at 80 °C (B), autoclaving at 120 °C (AC; C) or after dry-heating at 180 °C (DH; D). Scale bar = 50 μm. The inset shows the high-magnification images of sponge pores and scale bar represents 5 μm.

Full-size DOI: 10.7717/peerjmatsci.8/fig-1

RESULTS

Effects of heat treatments on the morphologies and secondary structures of SFSs

FESEM was conducted to examine the morphological difference between the porous structures of SFSs before and after heat treatments, as well as the difference between the three kinds of treatment (Fig. 1). Uniform porous structures were observed in all SFSs, indicating that heat treatment with or without water did not result in a morphological difference between SFSs.

To investigate the secondary structure of the protein molecules in the SFSs and in order to assess any structural changes resulting from the heat treatments, SFSs before and after the heat treatment were analyzed using ^{13}C CP/MAS NMR. The focus of the analysis was on the C_α and C_β peaks of Ala and Ser residues because these peaks are sensitive to structural changes and are relatively stronger and better resolved. Peak assignments were made by comparing the chemical shifts observed in the spectra of the peptides and those

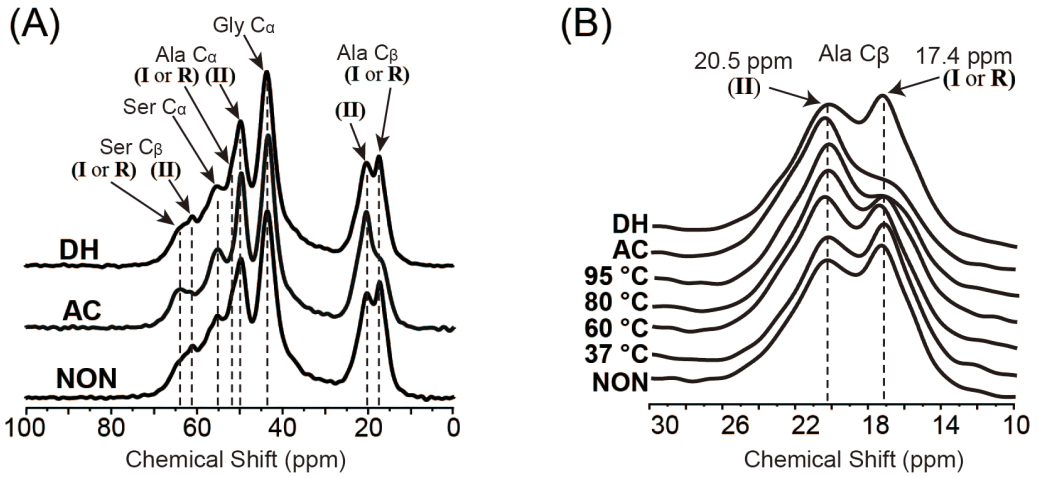

Figure 2 **NMR spectra of SFSs.** (A) ^{13}C CP/MAS NMR spectra of NON, AC and DH. (B) An expansion of the Ala C_β peak region (10–30 ppm) of the spectra of NON, wet-heated SFSs treated at 37 °C, 60 °C, 80 °C and 95 °C for 6 h, AC and DH. Arrows indicate the peaks of silk I (I), silk II (II) and random coil (R).

Full-size DOI: 10.7717/peerjmatsci.8/fig-2

of the other silk fibers (obtained from silkworms, spiders, etc.) in solution and the solid state. Figure 2A shows the C_α and C_β regions of the protein molecules in the ^{13}C CP/MAS NMR spectra of NON, AC and DH. The NMR spectrum of DH was very similar to that of NON, and the AC spectrum differed markedly. An expansion of the Ala C_β peak area of the heated SFSs is shown in Fig. 2B. An independent peak for Ala C_β was used to determine the structure of the fibroin molecules because of a large chemical shift in the structure (*Saitô, Tuzi & Naito, 1998*). The peaks at 17.4 and 20.5 ppm in Fig. 2B represent chemical shifts attributable to Ala in silk I and silk II structures, respectively. The intensity of the peak at 17.4 ppm decreased with the increasing treatment temperatures in the wet-treated SFSs, although AC exhibited only a small shoulder. In contrast, the peaks at 20.5 ppm that were attributable to silk II increased with increasing wet-heating temperatures. No structural changes were observed in DH even after the SFSs were heated above 120 °C, as described above (DH and NON in Fig. 2A).

To compare the effects of heat treatments on the SFS structure in detail, the ratio of silk II to silk I (II/I) was determined from the peak intensities of Ala C_β and plotted (Fig. 3) (*Kim et al., 2003*; *Zhou et al., 2004*). Structural changes from silk I to silk II were observed in SFSs wet-heated at 95 °C, which reached a plateau at around 30 min (Fig. 3A). When SFSs were wet-heated at 37 °C, 50 ° C, 60 °C, 80 °C, 95 ° C and 121 °C (AC) for 360 min, the II/I ratios were 0.92, 0.93, 1.06, 1.25, 1.55 and 1.64 respectively, indicating that the heat treatments in the presence of water induced structural changes from silk I to silk II (Fig. 3B). The II/I ratios for all of the SFSs in this temperature titration plateaued within the 360 min treatment time. The transformation from silk I to silk II occurred above 60 °C, and the II/I ratio increased with increasing temperature, with the highest II/I ration occurring in the autoclaved SFSs. Fibroin films have been reported to exhibit structural changes from random coils to silk I (and subsequently to silk II), which occurs

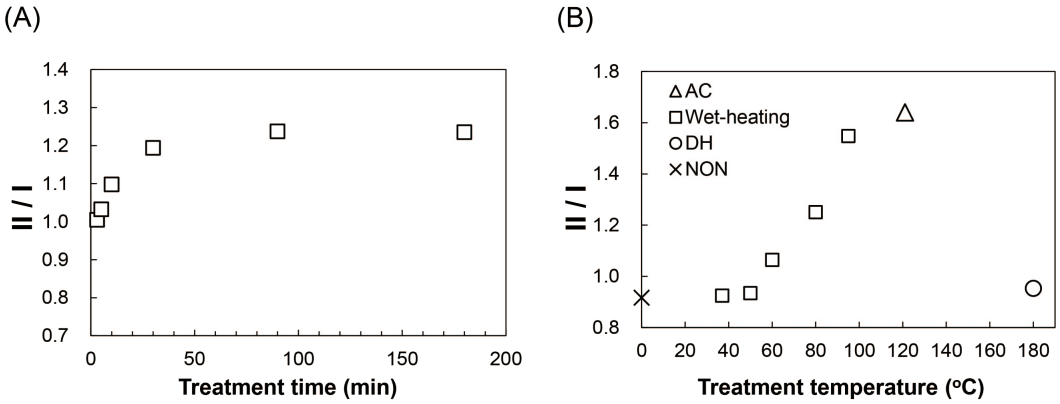

Figure 3 The influence of thermal treatments on the secondary structure of SFSs. Silk II: silk I ratios (II/I) of the intensities of NMR peaks attributable to Ala C_β for the wet-treated SFSs at 95 °C as a function of treatment time (A), and for the wet-heated (□), autoclaved (△), dry-heated (○) and non-treated (×) SFSs (B).

Full-size DOI: 10.7717/peerjmatsci.8/fig-3

in water at > 70 °C (*Magoshi et al., 1979*). Moreover, this transformation in films occurred in water even below 60 °C, whereas here, no transformation was observed in the SFS in water below 60 °C. Autoclave sterilization (exposure to steam at 121 °C for 20 min) of SFS also induced structural changes, as evident from the marked differences between the spectra shown in Fig. 2, indicating that the conformational transition from silk I to silk II occurs during autoclave treatment. In contrast, the ratio of DH was 0.95, which is close to the ratio of 0.92 for NON, suggesting that no structural changes occurred during the dry-heating treatment.

Properties of heated SFSs

Thermogravimetry (TG) curves of SFSs are shown in Fig. 4A. Following dehydration-induced weight loss at temperatures up to 180 °C, additional weight loss was also observed above 200 °C because of thermal degradation. Next, sponge samples were rapidly heated (100 °C/min) to an elevated temperature (after heating to 100 °C for removing residual absorbed moisture), and their weight loss due to thermal degradation was measured over time (Fig. 4B). The weights of SFSs heated to 180.5 °C and 190.2 °C remained unchanged over 180 min.

Maximum forces at break for heat-treated SFSs were quite similar as shown in Fig. 5. This result was consistent with the fact that there was no significant difference in morphology due to heat treatment conditions as described in Fig. 1.

Interactions with cells

Figure 6 shows the proliferation of NIH/3T3 cells cultured on AC and DH over 120 h. The calculated doubling times (from 24 h to 120 h) were 26 h (AC) and 34 h (DH) and were significantly different ($P < 0.005$, $n = 3$). However, both AC and DH contained similar cell numbers 168 h after seeding. Since both sponges were autoclaved and both dry-heating methods used the same pore size (Fig. 1), it appears that different structures of fibroin molecules affected the doubling times of fibroblast at early stages in culture.

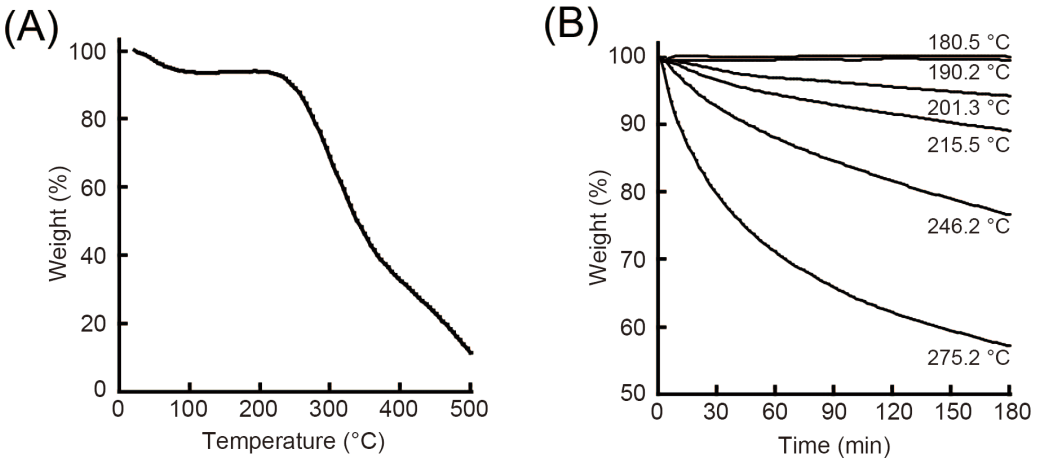

Figure 4 Thermal analysis of SFSs. Thermogravimetry and weight loss curves (%) of SFSs as a function of temperature at a heating rate of 3 °C/min (A). Weight loss (%) of SFSs due to thermal degradation at various temperatures under air flow as a function of time (B).

Full-size DOI: 10.7717/peerjmatsci.8/fig-4

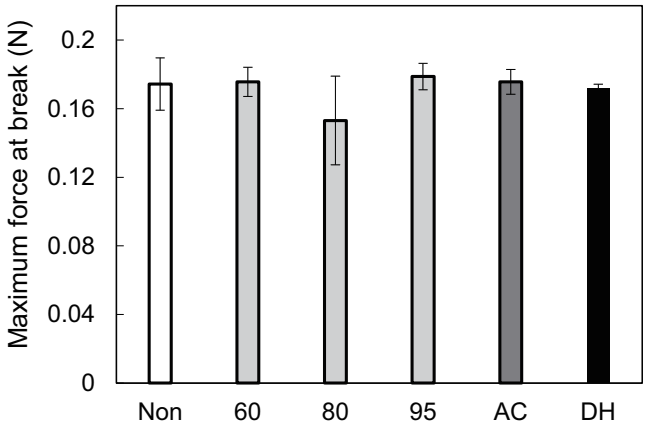

Figure 5 The maximum force at break of treated SFSs. Wet SFSs were stretched at five mm/min head speed using a 50 N load cell.

Full-size DOI: 10.7717/peerjmatsci.8/fig-5

To evaluate cell functions apart from proliferation, cell motilities were also measured quantitatively using single-cell tracking with time-lapse image capture coupled to computer image analysis. Cell migration is known to heavily depend on the structure and properties of the extracellular matrix (ECM) (*Li et al., 2004*). Fibroin-coated glass was prepared in order to mimic AC and DH surfaces and was used because of the difficulty inherent in measuring cellular migration in the confines of the three-dimensional structure of the SFSs. Figure 7 shows the FTIR-ATR spectra of the AC- and DH-mimicking surfaces. To analyze the contents of each structure in the mimicking surfaces, the amide I band was deconvoluted into individual bands by Gaussian curve-fitting (*Tretinnikov & Tamada, 2001*; *Hu, Kaplan & Cebe, 2006*; (*Dong, Huang & Caughey, 1990*). Bands centered at around 1,610, 1,619, 1,625, 1,633, 1,642, 1,651, 1,659 and 1,680 cm^{-1} were assigned to Tyr side

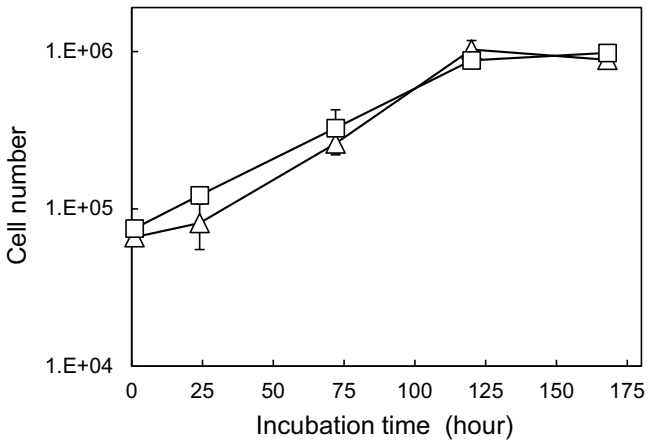

Figure 6 Cell proliferation curves on SFSs. Cell number on autoclaved (AC, △) and dry-heated (DH, □) SFSs. Cell numbers in the three SFS samples were averaged at each time point.
Full-size DOI: 10.7717/peerjmatsci.8/fig-6

Table 2 Contents of β-sheets, α-helices, random coils and turns from the intensities of ATR-IR peaks attributable to amide I in AC-mimicking and DH-mimicking surfaces.

Mimicking surface	Contents (%)			
	β-sheet	random coil	α-helix	turn
DH	29.6	26.3	19.4	24.7
AC	51.3	17.0	16.3	15.4

chain/aggregated strand (SC), aggregated β-strand/ β-sheet (B), β-sheet (B), β-sheet (B), random coil/extended chain (R), α-helix (A) and turn (T), respectively. A band centered at 1,700 cm^{-1} and assigned to β-sheet (B) was detected in AC- mimicking surfaces. Contents of β-sheets, α-helices, random coils and turns obtained from amide I band measurements are shown in Table 2. Compared to the structure contents of DH-treated mimicking surfaces, AC-mimicking surfaces clearly exhibited higher levels of β-sheet structure. These results demonstrate that secondary structures in AC-mimicking surfaces changed to β-sheet upon autoclave treatment, similarly to the structural changes in SFSs detected by NMR measurements. This evaluation indicated that AC-mimicking and DH-mimicking surfaces could indeed mimic autoclaved and dry-heated SFSs (AC and DH), although the absolute values of silk I or silk II contents differed slightly. The contact angle for uncoated glass was 37.7 ± 3.4°, which increased in fibroin-coated surfaces. The AC-mimicking surfaces had a contact angle of 49.1 ± 9.2° and were found to be more hydrophilic than the DH-mimicking surfaces (78.5 ± 0.4°). Figure 8 shows the cell migration on the mimicking surface. The movements of the fibroblasts 23 h after attachment to AC- and DH-mimicking surfaces were 747 and 588 μm, respectively. Thus, cell motility was slightly higher on AC-mimicking surfaces.

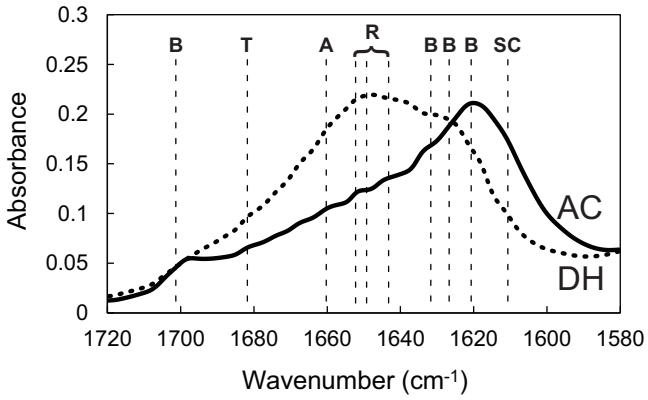

Figure 7 FTIR-ATR spectra of SFSs. FTIR-ATR spectra in the amide I region of AC-mimicking (solid line) and DH-mimicking (dotted line) surfaces. The vertical dashed lines delimit the regions assigned to secondary structures: B, β-sheet, T, turn, A, α-helix, R, random, SC, Tyr side chain/aggregated strand.
Full-size DOI: 10.7717/peerjmatsci.8/fig-7

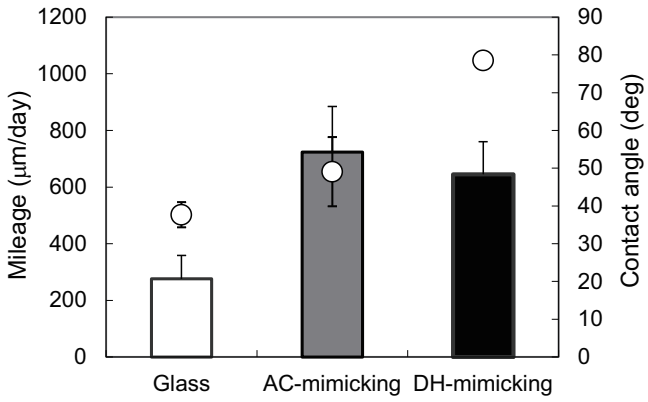

Figure 8 Evaluations of mimicking surfaces. Migration distances of NIH/3T3 cultured on AC-mimicking (grey bar), DH-mimicking (black bar) and glass surfaces (white bar). Contact angles (○) of mimics were measured by sessile drop. $^{*}P = 0.22$.
Full-size DOI: 10.7717/peerjmatsci.8/fig-8

DISCUSSION

The transformation from silk I to silk II occurred at temperatures > 60 °C, and II/I ratio increased with increasing temperature, with the highest II/I being observed in the autoclave treatment. In contrast, no structural change of SFSs was induced by dry heating (Fig. 3B). Dry-heat treatment, such as that used in the sterilization of polymeric biomaterials, generally causes yellowing because of thermal decomposition (*Bos et al., 2005*); thus, dry-heating treatments are usually used for sterilization of metals (*Thierry et al., 2000*). NMR and TG studies revealed high structural resistance of silk fibroins to elevated temperatures in the absence of water, and the structure of the silk fibroin molecules was found to be stable even after dry heating up to 190 °C. Figure 4 shows the thermostability of the fibroin molecules in SFSs, indicating heat resistance up to 190 °C, although thermal degradation occurred at temperatures above 200 °C. The solid-state NMR spectrum of DH was identical

to that of NON (Fig. 2), indicating that no structural changes occurred during dry heating (180 °C for 180 min). These results indicate that our SFSs are heat-resistant up to 180 °C for about 180 min. This is important because samples have been exposed to hot air at 180 °C for over 30 min in dry-heat sterilization processes (*Hattori et al., 2011*; *Ploux et al., 2009*). The above results clearly show that these SFSs can undergo dry sterilization with thermal, structural and color stabilities similar to those of hornet silk materials (*Kameda & Aratani, 2011*).

Hofmann et al. and Rnjak-Kovacina et al. reported that porous silk fibroin scaffolds remained structurally intact after sterilization treatments that included autoclaving (*Hofmann et al., 2014*) and dry heat (*Rnjak-Kovacina et al., 2015*). Their results were different from ours because, in our study, obvious structural changes were seen in SFSs that underwent autoclaving (Figs. 2 and 3). This difference could be explained by a number of reasons. Hofmann et al. prepared porous scaffolds using the salt leaching method, which was followed by MeOH treatments. The scaffolds of Rnjak-Kovacina et al. were obtained by freeze-drying and exposure to water vapor. The water-insoluble silk II structures in their scaffolds were thought to plateau before the sterilization treatments. Presumably, there were some differences between the initial structures in Hofmann's porous scaffolds (silk II rich) and our sponges. MeOH and water vapor treatments are necessary for converting their scaffolds to insoluble structures, after which silk I (or random coils) transforms to silk II and transitions from a soluble to an insoluble form. The β-sheet content of the silk II in Hofmann's porous scaffolds probably reached a plateau prior to the autoclaving treatment, since results from IR measurements of all of the MeOH-treated porous scaffolds clearly indicated that MeOH induced significant structural changes from silk I to β-sheets. Other porous scaffolds prepared by generic methods (e.g., freeze-drying, salt leaching or gas formation) require similar treatment prior to autoclaving (*Hofmann et al., 2014*; *Rnjak-Kovacina et al., 2015*; *Nazarov, Jin & Kaplan, 2004*). In contrast, the SFSs that we developed easily crystallized to form insoluble silk fibroins (*Tamada, 2005*) and did not require MeOH treatments prior to sterilization. In addition, our unpublished data show that autoclave treatment at 121 °C for $>$ 40 min induced no further structural changes, as compared to some of the changes seen at 121 °C for 20 min. These results show that the structural changes (from silk I/random coil to silk II) in the sponges that we developed almost reached a plateau in 20 min. We speculate that the somewhat dissimilar initial proportions of silk I/random coil and silk II structures might have induced dissimilar behaviors in the silk fibroin scaffolds (e.g., the structural changes or the interactions with cells). Properties of silk fibroin-based materials also seem to vary according to the methods used in their preparation. Our results thus highlight the influences of some sterilization methods on structural changes and the resulting changes of cellular functions.

Cells cultured on DH exhibited slight slower proliferations in early stages than the cells cultured on the AC (Fig. 6). The study on the temperature-dependent structural changes of fibroin molecules in films by *Hu et al. (2011)*. indicated that β-sheet contents in fibroin affect the substrate adherence and proliferation of human mesenchymal stem cells. Rnjak-Kovacina et al. reported that autoclaved scaffolds promoted faster proliferation than other sterilized scaffolds, including dry-heated scaffolds, for 1 to 5 days after seeding.

However, similar cell numbers were observed in both autoclaved and dry-heat-treated scaffolds at 7 days after cell seeding. These results are consistent with our results on the cell proliferation of fibroblasts cultured on AC and DH. Our previous study demonstrated that the fibroin surface exhibits a higher potential for enhancing cell mobility and the production of extracellular matrix than do collagen and fibronectin surfaces (*Hashimoto et al., 2013*). Two fibroin-mimicking surfaces with different structure contents (Fig. 7 and Table 2) exhibited different contact angles and slightly different cell motilities (Fig. 8). Thus, surface contact angles as well as the corresponding structures of silk fibroin molecules seemed to affect cell mobility.

George et al. (2013) also compared some sterilization methods using fibroin films. Their results revealed that fibroin films sterilized by autoclaving contained a higher β-sheet content compared to films treated by gamma irradiation or with ethanol. Cell attachment was only observed in the crevices of the autoclaved film surface, and cells attached uniformly to the fibroin surfaces treated with gamma radiation and ethanol. The present study indicates that no structural changes or thermal decomposition was observed in dry-heated fibroin molecules (Figs. 3 and 4) and that there were no significant differences between the appearances of the AC- and DH-mimicking surfaces, although slight differences in cell proliferation were observed (Fig. 6). The interactions between biomaterials and cells are related to the contact angles of the material surfaces. Results from contact angles (Fig. 8) revealed that autoclave treatment increased the wettability of the fibroin surfaces. One of the authors has reported that fibroin films that have the highest β-sheet content also display a higher electron-donor (γs-) parameter for surface energy than films containing lower amounts of β-sheets (*Tretinnikov & Tamada, 2001*). Different secondary structures induced different surface properties of the fibroin-based biomaterials, such as contact angle and the surface energy. Various interactions between these biomaterials and cells were mediated by these different properties. Thus, we surmise that the seeded cells might recognize the microarchitecture of the fibroin surface.

The influence of temperature on the near-surface structure of cast fibroin films has been investigated using FTIR-ATR (*Tretinnikov & Tamada, 2001*). These investigations indicated that the near-surface conformations were quite different from those of the bulk. The solid-state NMR measurements of the fibroin molecules revealed details about both surface and bulk structures and indicated that mimicking surfaces exhibited a similar tendency in secondary structures as bulk structure in sponges. Analyses of the local structures on the surfaces of SFSs seem important, since cells initially interact with the near surfaces of biomaterials. The characteristic structures of the fibroin surfaces of the aforementioned biomaterials facilitated specific cell attachment; cell proliferation was also enhanced for the same reason. Further investigation into these structural changes might reveal the relationship between the structures of fibroin molecules and their interactions with cells or tissues.

CONCLUSIONS

The influences of heat treatment in the presence and absence of water on the structural changes of SFSs were investigated. Wet-heating treatment of SFSs at temperatures >

60 °C induced structural changes from silk I to silk II, and these changes increased with increasing temperatures. In contrast, in the absence of water, dry heating up to 180 °C did not induce structural changes in the fibroin molecules. In the present study, we found almost similar cellular behaviors on two different silk fibroin surfaces. These results indicate that both autoclaving and dry heating are viable alternatives for the sterilization of fibroin biomaterials. In particular, dry heating also helps in maintaining the overall structural stability of the sterilized silk fibroin-based biomaterials.

ADDITIONAL INFORMATION AND DECLARATIONS

Funding

This work was supported by the Agri-Health Translational Research Project and by the research and development project for application in promoting a new policy for Agriculture Forestry and Fisheries and the individual research expense of Nara Women's University. The funders had no role in study design, data collection and analysis, decision to publish, or preparation of the manuscript.

Grant Disclosures

The following grant information was disclosed by the authors:
Agri-Health Translational Research Project.
Nara Women's University.

Competing Interests

The authors declare there are no competing interests.

Author Contributions

- Tomoko Hashimoto conceived and designed the experiments, performed the experiments, analyzed the data, performed the computation work, prepared figures and/or tables, authored or reviewed drafts of the paper, and approved the final draft.
- Yuka Nakamura performed the experiments, analyzed the data, prepared figures and/or tables, and approved the final draft.
- Yasushi Tamada and Hiromichi Kurosu analyzed the data, authored or reviewed drafts of the paper, and approved the final draft.
- Tsunenori Kameda conceived and designed the experiments, performed the experiments, analyzed the data, performed the computation work, prepared figures and/or tables, authored or reviewed drafts of the paper, and approved the final draft.

Data Availability

The following information was supplied regarding data availability:

The raw measurements are available as Supplementary Files.

Supplemental Information

Supplemental information for this article can be found online at http://dx.doi.org/10.7717/peerj-matsci.8#supplemental-information.

REFERENCES

Archodoulaki VM, Koch T, Rodriguez A, Seidler S. 2011. Influence of different sterilization procedures on the morphological parameters and mechanical properties of ultra-high-molecular-weight polyethylene. *Journal of Applied Polymer Science* **120**:1875–1884 DOI 10.1002/app.31437.

Aznar-Cervantes SD, Pagan A, Monteagudo Santesteban B, Cenis JL. 2019. Effect of different cocoon stifling methods on the properties of silk fibroin biomaterials. *Scientific Reports* **9**:6703 DOI 10.1038/s41598-019-43134-5.

Bat E, Plantinga JA, Harmsen MC, Van Luyn MJA, Zhang Z, Grijpma DW, Feijen J. 2008. Trimethylene carbonate and ϵ-caprolactone based (co)polymer networks: mechanical properties and enzymatic degradation. *Biomacromolecules* **9**:3208–3215 DOI 10.1021/bm8007988.

Bos GW, Hennink WE, Brouwer LA, Den Otter W, Veldhuis TFJ, Van Nostrum CF, Van Luyn MJA. 2005. Tissue reactions of in situ formed dextran hydrogels crosslinked by stereocomplex formation after subcutaneous implantation in rats. *Biomaterials* **26**:3901–3909 DOI 10.1016/j.biomaterials.2004.10.008.

Cheng X, Deng D, Chen L, Jansen JA, Leeuwenburgh SGC, Yang F. 2020. Electrodeposited assembly of additive-free silk fibroin coating from pre-assembled nanospheres for drug delivery. *ACS Applied Materials & Interfaces* **12**:12018–12029 DOI 10.1021/acsami.9b21808.

Dong A, Huang P, Caughey WS. 1990. Protein secondary structures in water from second-derivative amide I infrared spectra. *Biochemistry* **29**:3303–3308 DOI 10.1021/bi00465a022.

Fan L, Wang H, Zhang K, He C, Cai Z, Mo X. 2012. Regenerated silk fibroin nanofibrous matrices treated with 75% ethanol vapor for tissue-engineering applications. *Journal of Biomaterials Science, Polymer Edition* **23**:497–508 DOI 10.1163/092050610X552771.

George KA, Shadforth AMA, Chirila TV, Laurent MJ, Stephenson S-A, Edwards GA, Madden PW, Hutmacher DW, Harkin DG. 2013. Effect of the sterilization method on the properties of bombyx mori silk fibroin films. *Materials Science and Engineering: C* **33**:668–674 DOI 10.1016/j.msec.2012.10.016.

Hashimoto T, Kojima K, Otaka A, Takeda YS, Tomita N, Tamada Y. 2013. Quantitative evaluation of fibroblast migration on a silk fibroin surface and tgfbi gene expression. *Journal of Biomaterials Science, Polymer Edition* **24**:158–169 DOI 10.1163/156856212X629025.

Hattori S, Terada D, Bintang AB, Honda T, Yoshikawa C, Teramoto H, Kameda T, Tamada Y, Kobayashi H. 2011. Influence of sterilisations on silk protein-based materials. *Bioinspired, Biomimetic and Nanobiomaterials* **1**:195–199.

Hofmann S, Stok KS, Kohler T, Meinel AJ, Müller R. 2014. Effect of sterilization on structural and material properties of 3-d silk fibroin scaffolds. *Acta Biomaterialia* **10**:308–317 DOI 10.1016/j.actbio.2013.08.035.

Holy CE, Cheng C, Davies JE, Shoichet MS. 2000. Optimizing the sterilization of plga scaffolds for use in tissue engineering. *Biomaterials* **22**:25–31 DOI 10.1016/S0142-9612(00)00136-8.

Hu X, Kaplan D, Cebe P. 2006. Determining beta-sheet crystallinity in fibrous proteins by thermal analysis and infrared spectroscopy. *Macromolecules* **39**:6161–6170 DOI 10.1021/ma0610109.

Hu X, Kaplan D, Cebe P. 2008. Dynamic protein −water relationships during β-sheet formation. *Macromolecules* **41**:3939–3948 DOI 10.1021/ma071551d.

Hu X, Shmelev K, Sun L, Gil E-S, Park S-H, Cebe P, Kaplan DL. 2011. Regulation of silk material structure by temperature-controlled water vapor annealing. *Biomacromolecules* **12**:1686–1696 DOI 10.1021/bm200062a.

Jeong L, Lee KY, Liu JW, Park WH. 2006. Time-resolved structural investigation of regenerated silk fibroin nanofibers treated with solvent vapor. *International Journal of Biological Macromolecules* **38**:140–144 DOI 10.1016/j.ijbiomac.2006.02.009.

Jiang T, Zhou P. 2011. Environment-induced silk fibroin conformation based on the magnetic resonance spectroscopy. InTech 354–372.

Kameda T, Aratani E. 2011. Production and characterizations of tubes from hornet (*vespa*) silk. *Journal of Insect Biotechnology and Sericology* **80**:109–116.

Kameda T, Hashimoto T, Tamada Y. 2011. Effects of supercooling and organic solvent on the formation of a silk sponge with porous 3-D structure, and its dynamical and structural characterization using solid-state NMR. *Journal of Materials Science* **46**:7923–7930 DOI 10.1007/s10853-011-5925-6.

Kaneko A, Tamada Y, Hirai S, Kuzuya T, Hashimoto T. 2012. Characterization of a silk-resinified compact fabricated using a pulse-energizing sintering device. *Macromolecular Materials and Engineering* **297**:272–278 DOI 10.1002/mame.201100112.

Kawakami M, Tomita N, Shimada Y, Yamamoto K, Tamada Y, Kachi N, Suguro T. 2011. Chondrocyte distribution and cartilage regeneration in silk fibroin sponge. *Bio-medical Materials and Engineering* **21**:53–61 DOI 10.3233/BME-2011-0656.

Kim SH, Nam YS, Lee TS, Park WH. 2003. Silk fibroin nanofiber, electrospinning, properties, and structure. *Polymer Journal* **35**:185–190 DOI 10.1295/polymj.35.185.

Kopp A, Smeets R, Gosau M, Kröger N, Fuest S, Köpf M, Kruse M, Krieger J, Rutkowski R, Henningsen A, Burg S. 2020. Effect of process parameters on additive-free electrospinning of regenerated silk fibroin nonwovens. *Bioactive Materials* **5**:241–252 DOI 10.1016/j.bioactmat.2020.01.010.

Lawrence B, Omenetto F, Chui K, Kaplan D. 2008. Processing methods to control silk fibroin film biomaterial features. *Journal of Materials Science* **43**:6967–6985 DOI 10.1007/s10853-008-2961-y.

Lee DH, Tripathy N, Shin JH, Song JE, Cha JG, Min KD, Park CH, Khang G. 2017. Enhanced osteogenesis of β-tricalcium phosphate reinforced silk fibroin scaffold for bone tissue biofabrication. *International Journal of Biological Macromolecules* **95**:14–23 DOI 10.1016/j.ijbiomac.2016.11.002.

Li W, Fan J, Chen M, Guan S, Sawcer D, Bokoch GM, Woodley DT. 2004. Mechanism of human dermal fibroblast migration driven by type I collagen and

platelet-derived growth factor-BB. *Molecular Biology of the Cell* **15**:294–309 DOI 10.1091/mbc.e03-05-0352.

Luetchford KA, Chaudhuri JB, De Bank PA. 2020. Silk fibroin/gelatin microcarriers as scaffolds for bone tissue engineering. *Materials Science and Engineering: C* **106**:110116 DOI 10.1016/j.msec.2019.110116.

Magoshi J, Mizuide M, Magoshi Y, Takahashi K, Kubo M, Nakamura S. 1979. Physical properties and structure of silk, VI. Conformational changes in silk fibroin induced by immersion in water at 2 to 130 °C. *Journal of Polymer Science: Polymer Physics Edition* **17**:515–520.

Mao B, Liu C, Zheng W, Li X, Ge R, Shen H, Guo X, Lian Q, Shen X, Li C. 2018. Cyclic cRGDfk peptide and Chlorin e6 functionalized silk fibroin nanoparticles for targeted drug delivery and photodynamic therapy. *Biomaterials* **161**:306–320 DOI 10.1016/j.biomaterials.2018.01.045.

Marreco PR, Moreira PdL, Genari SC, Moraes ÂM. 2004. Effects of different sterilization methods on the morphology, mechanical properties, and cytotoxicity of chitosan membranes used as wound dressings. *Journal of Biomedical Materials Research Part B: Applied Biomaterials* **71B**:268–277 DOI 10.1002/jbm.b.30081.

Matsumoto A, Chen J, Collette AL, Kim U-J, Altman GH, Cebe P, Kaplan DL. 2006. Mechanisms of silk fibroin sol −gel transitions. *The Journal of Physical Chemistry B* **110**:21630–21638 DOI 10.1021/jp056350v.

Min B-M, Jeong L, Lee KY, Park WH. 2006. Regenerated silk fibroin nanofibers: water vapor-induced structural changes and their effects on the behavior of normal human cells. *Macromolecular Bioscience* **6**:285–292 DOI 10.1002/mabi.200500246.

Min B-M, Jeong L, Nam YS, Kim J-M, Kim JY, Park WH. 2004. Formation of silk fibroin matrices with different texture and its cellular response to normal human keratinocytes. *International Journal of Biological Macromolecules* **34**:223–230.

Nazarov R, Jin H-J, Kaplan DL. 2004. Porous 3-D scaffolds from regenerated silk fibroin. *Biomacromolecules* **5**:718–726 DOI 10.1021/bm034327e.

Noah EM, Chen J, Jiao X, Heschel I, Pallua N. 2002. Impact of sterilization on the porous design and cell behavior in collagen sponges prepared for tissue engineering. *Biomaterials* **23**:2855–2861 DOI 10.1016/S0142-9612(01)00412-4.

Oliveira AL, Sun L, Kim HJ, Hu X, Rice W, Kluge J, Reis RL, Kaplan DL. 2012. Aligned silk-based 3-d architectures for contact guidance in tissue engineering. *Acta Biomaterialia* **8**:1530–1542 DOI 10.1016/j.actbio.2011.12.015.

Ploux L, Anselme K, Dirani A, Ponche A, Soppera O, Roucoules V. 2009. Opposite responses of cells and bacteria to micro/nanopatterned surfaces prepared by pulsed plasma polymerization and UV-irradiation. *Langmuir* **25**:8161–8169 DOI 10.1021/la900457f.

Rnjak-Kovacina J, DesRochers TM, Burke KA, Kaplan DL. 2015. The effect of sterilization on silk fibroin biomaterial properties. *Macromolecular Bioscience* **15**:861–874 DOI 10.1002/mabi.201500013.

Saitô H, Tuzi S, Naito A. 1998. polysaccharides and biological systems. In: Ando I Asakura T, ed. *Studies in physical and theoretical chemistry*. Amsterdam, Netherlands: Elsevier, 891–921.

Sionkowska A, Planecka A. 2011. The influence of UV radiation on silk fibroin. *Polymer Degradation and Stability* **96**:523–528 DOI 10.1016/j.polymdegradstab.2011.01.001.

Tamada Y. 2003. Sulfation of silk fibroin by sulfuric acid and anticoagulant activity. *Journal of Applied Polymer Science* **87**:2377–2382 DOI 10.1002/app.12022.

Tamada Y. 2005. New process to form a silk fibroin porous 3-d structure. *Biomacromolecules* **6**:3100–3106 DOI 10.1021/bm050431f.

Tamada Y, Ikada Y. 1994. Fibroblast growth on polymer surfaces and biosynthesis of collagen. *Journal of Biomedical Materials Research* **28**:783–789 DOI 10.1002/jbm.820280705.

Thierry B, Tabrizian M, Savadogo O, Yahia LH. 2000. Effects of sterilization processes on niti alloy: surface characterization. *Journal of Biomedical Materials Research* **49**:88–98 DOI 10.1002/(SICI)1097-4636(200001)49:1<88::AID-JBM11>3.0.CO;2-I.

Tretinnikov ON, Tamada Y. 2001. Influence of casting temperature on the near-surface structure and wettability of cast silk fibroin films. *Langmuir* **17**:7406–7413 DOI 10.1021/la010791y.

Voggenreiter G, Ascherl R, Blümel G, Schmit-Neuerburg KP. 1994. Effects of preservation and sterilization on cortical bone grafts. *Archives of Orthopaedic and Trauma Surgery* **113**:294–296 DOI 10.1007/BF00443821.

Yavuz B, Morgan JL, Herrera C, Harrington K, Perez-Ramirez B, LiWang PJ, Kaplan DL. 2019. Sustained release silk fibroin discs: antibody and protein delivery for HIV prevention. *Journal of Controlled Release* **301**:1–12 DOI 10.1016/j.jconrel.2019.03.001.

Zhang C, Zhang Y, Shao H, Hu X. 2016. Hybrid silk fibers dry-spun from regenerated silk fibroin/graphene oxide aqueous solutions. *ACS Applied Materials & Interfaces* **8**:3349–3358 DOI 10.1021/acsami.5b11245.

Zhou P, Xie X, Knight DP, Zong X-H, Deng F, Yao W-H. 2004. Effects of pH and calcium ions on the conformational transitions in silk fibroin using 2D raman correlation spectroscopy and ^{13}C solid-state NMR. *Biochemistry* **43**:11302–11311 DOI 10.1021/bi049344i.

Zuluaga-Vélez A, Cómbita-Merchán DF, Buitrago-Sierra R, Santa JF, Aguilar-Fernández E, Sepúlveda-Arias JC. 2019. Silk fibroin hydrogels from the Colombian silkworm Bombyx mori L: evaluation of physicochemical properties. *PLOS ONE* **14**:e021330.